**Adilkhan Kapanov**

Thesis Defense | 01.05.2025

# External Object Detection in Wireless Power Transfer for EV

Adilkhan Kapanov | 201785607

Supervisor: Mehdi Bagheri
Co-supervisor: Annie Ng

NAZARBAYEV UNIVERSITY

# Table of contents

# Introduction

Transferring energy from a single source to the load without the use of wires is known as wireless power transfer (WPT). There are two types of WPT: near-field WPT and far-field or microwave power transfer [1, 2].

Inductive Power Transfer (IPT) is the process of transferring power through magnetic fields. The primary coil's alternating current generates an alternating current on the receiver coil side [3, 4].

Resonant-Coupled IPT (RC-IPT) is an enhanced version of IPT that performs best over midrange distances when compared to other WPT techniques.

WPT systems have their own problems, one of which is when an external object (EO), like keys, coins, or tiny animals, is present in the system's operating area. Due to the working conditions of the system, which include high power levels and the presence of strong AC electromagnetic fields between coils, the presence of EO may lead to potentially dangerous situations [5].

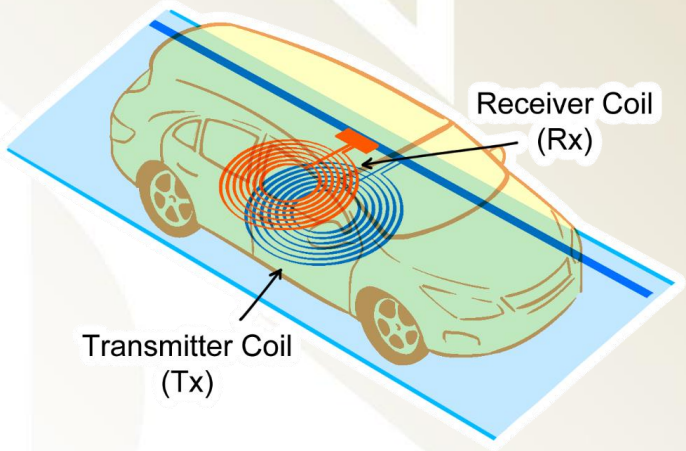


Fig 1. Wireless power transfer system for an electric vehicle.

# Introduction

External object detection (EOD) techniques are being researched to stop these situations. Metal object detection (MOD) and living object detection (LOD) are two types of EOD techniques that are based on the physical characteristics of the object [6].

This research study proposes sensing coil-based method of external object detection and its sensitivity analysis over the range of frequencies. The project aims to provide important insights for the creation of future WPT systems that can function reliably and effectively in dynamic frequency situations by tackling these goals.

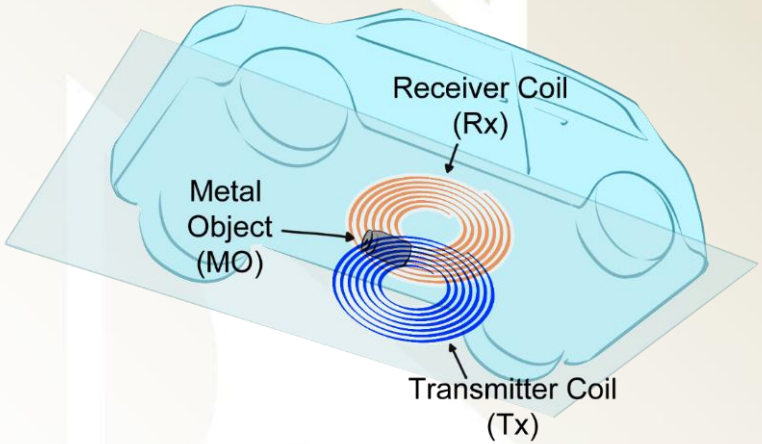


Fig 2. External metal object in the WPT system for an EV.

# Literature Review

**Table 1. The comparison of MOD methods.**

| MOD methods | Operating principle | Advantages | Disadvantages |
|---|---|---|---|
| **Parameter-based** | Examining the electrical properties of the system resulting from variations in the self-inductance of the coils | • The system is self-sustaining, necessitating no supplementary equipment or costs;<br>• High detection time. | • Challenging to recognize MOs in misalignment situations;<br>• Inappropriate for high-power applications. |
| **Sensing coil-based** | Through the examination of the induced voltage, induced current, and impedance of the sensing coil | • Tolerance for misalignment;<br>• Capability to detect small-sized MOs;<br>• Functions at various power levels. | • Necessity for consistent design to eradicate blind spots. |
| **Sensor-based** | Assess or observe variations in the physical characteristics of a system utilizing external sources. | • Extensive detection range;<br>• Functions effectively despite misalignment;<br>• High accuracy. | • Elevated costs compared to alternatives;<br>• Performance impacted by external factors;<br>• Complexity in circuit implementation due to size. |

# Research Methodology and Modelling

**WPT-EOD Method**

EOD method applying five open-circuited sensing coils to modify existing transmitter current is used. In this regard, geometric parameters and sense coil voltages, which capture the electromagnetic couplings between the transmitter, receiver, and sense coils are necessary for the modification.

The sequent error $\epsilon_D$, which arises from a foreign object due to additional electromagnetic coupling, is useful as a detection metric. The genuine Tx coil current $I_T$ is measured independently and compared to the reconstructed Tx coil current $I_t$ [7, 8]:

$$\epsilon_D = \left| \frac{I_T - I_t}{I_T} \right| * 100(\%)$$

The main reason for choosing this method was because of its advantages over other methods, such as:

- Power level invariance, leading to the low-power startups before charging EV.
- The ability to identify EMOs in the cases of lateral misalignment up to 10 cm.
- The ability to detect EMOs within the operating area of the system with no blind areas.
- Reliance only on the transmitter side of the system.

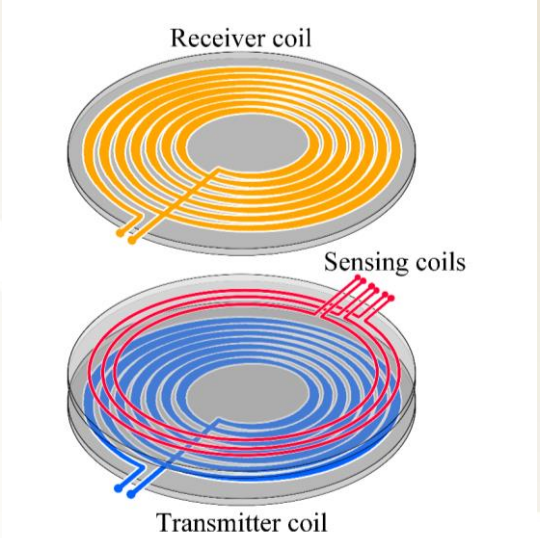


Fig 3. Schematic of the implementation of the sensing coil in WPT systems.

# Research Methodology and Modelling

**Modelling of WPT-EOD System**

Figure 4 shows a schematic of the proposed WPT-EOD system studied in [7]:

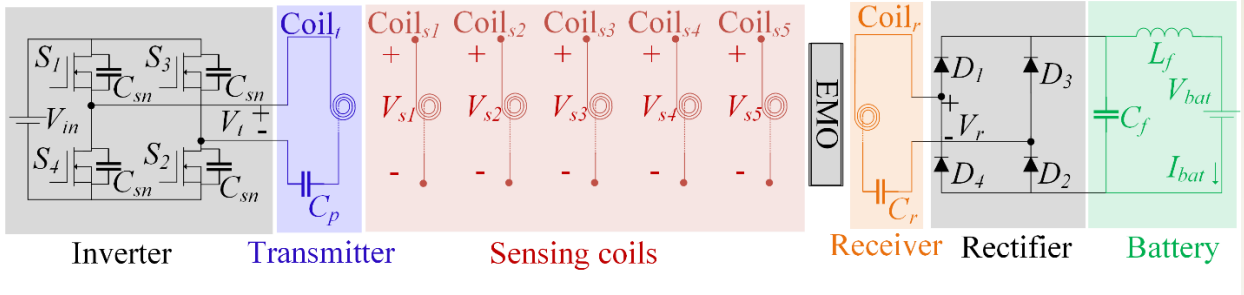


Fig 4. Schematic model and structure of the WPT-EOD system.

Series-series topology, that connects single capacitor in series to a magnetic coil at both transmitter and receiver side is used due to its widespread usage in IPT systems [9].

The planar spiral coil design was selected as the primary design because of its widespread use [10]. Note that Litz wires, namely the skin effect, reduce AC winding losses, which is the reason they employed rather than a single solid wire.

# Research Methodology and Modelling

$$\begin{bmatrix} V_t \\ \underbrace{V_{sx}}_{5\times1} \\ 0 \end{bmatrix} = \begin{bmatrix} Z_{t,t} & \underbrace{Z_{t,sx}}_{1\times5} & Z_{t,r} \\ \underbrace{Z_{sx,t}}_{5\times1} & \underbrace{Z_{sx,sx}}_{5\times5} & \underbrace{Z_{sx,r}}_{5\times1} \\ Z_{r,t} & \underbrace{Z_{r,sx}}_{1\times5} & Z_{r,r} \end{bmatrix} \begin{bmatrix} I_t \\ \underbrace{0}_{5\times1} \\ I_r \end{bmatrix}$$

$$Z_{t,t} = 2r_{DS} + R_t + \frac{1}{jw_sC_t} + jw_sL_t$$

$$Z_{r,r} = R_r + R_L + \frac{1}{jw_sC_r} + jw_sL_r \qquad Z_{t,sx} = [Z_{sx,t}]^T = [-jw_sM_{t,s1}, \dots, -jw_sM_{t,s5}]$$

$$Z_{t,r} = Z_{r,t} = -jw_sM_{t,r} \qquad Z_{sx,sx}(i,i) = jw_sL_{si} + R_{si}$$

$$Z_{sx,sx}(i,j)\Big|_{i\neq j} = Z_{sx,sx}(j,i)\Big|_{i\neq j} = jw_sM_{si,sj} \qquad Z_{sx,r} = [Z_{r,sx}]^T = [jw_sM_{s1,r}, \dots, jw_sM_{s5,r}]^T$$

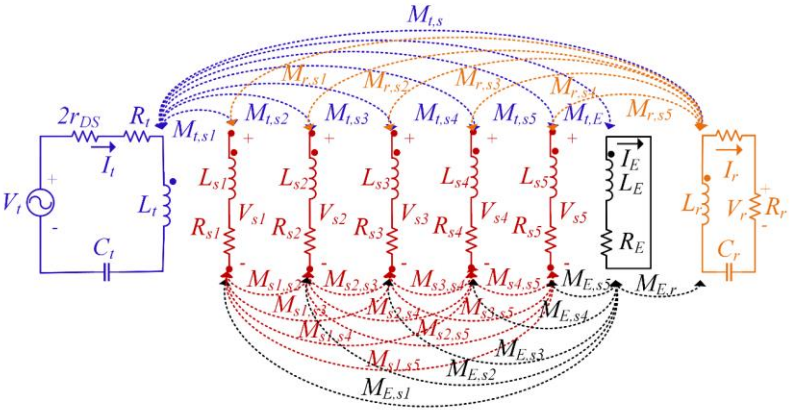


Fig 5. Equivalent electrical circuit of proposed resonant coupled wireless power transfer system with five sensing coils and external object.

# Research Methodology and Modelling

The equations for the sensing coil voltages $V_{s1}$, $V_{s2}$, $V_{s3}$, $V_{s4}$, $V_{s5}$ and inverter current $I_t$ is derived as follows:

$$V_{sx} = I_t Z_{sx,t} + 0 * Z_{sx,sx} + I_r Z_{sx,r} \qquad 0 = I_t Z_{r,t} + 0 * Z_{r,sx} + Z_{r,r} I_r \qquad I_r = -I_t \frac{Z_{r,t}}{Z_{r,r}} \qquad V_{sx} = [V_{s1}, V_{s2}, V_{s3}, V_{s4}, V_{s5}]^T$$

$$V_{sx} = I_t \left( \frac{Z_{sx,t} Z_{r,r} - Z_{r,t} Z_{sx,r}}{Z_{r,r}} \right)$$

Using linear combinations of every sense coil voltage, first, simplify the equations by introducing geometric parameter $a_x$, where $x$ corresponds to each one of the open circuited sense coil voltages and then derive transmitter current $I_t$:

$$a_x = \frac{Z_{sx,t} Z_{r,r} - Z_{r,t} Z_{sx,r}}{Z_{r,r}} \qquad I_t = \frac{1}{5} \sum_{i=1}^{5} V_{si} a_i = \frac{1}{5} (V_{s1} a_1 + V_{s2} a_2 + V_{s3} a_3 + V_{s4} a_4 + V_{s5} a_5)$$

# Research Methodology and Modelling

As for the case of the presence of EMO in the operating area of the system, the matrix is going to expand with the addition of the induced eddy current on EMO, denoted by $I_E$:

$$\begin{bmatrix} V_t \\ \underbrace{V_{sx}}_{5\times1} \\ 0 \\ 0 \end{bmatrix} = \begin{bmatrix} Z_{t,t} & \underbrace{Z_{t,sx}}_{1\times5} & Z_{t,r} & Z_{t,E} \\ \underbrace{Z_{sx,t}}_{5\times1} & \underbrace{Z_{sx,sx}}_{5\times5} & \underbrace{Z_{sx,r}}_{5\times1} & \underbrace{Z_{sx,E}}_{5\times1} \\ Z_{r,t} & \underbrace{Z_{r,sx}}_{1\times5} & Z_{r,r} & Z_{r,E} \\ Z_{E,t} & \underbrace{Z_{E,sx}}_{1\times5} & Z_{E,r} & Z_{E,E} \end{bmatrix} \begin{bmatrix} I_t \\ \underbrace{0}_{5\times1} \\ I_r \\ I_E \end{bmatrix}$$

$$I_E = -\frac{Z_{E,t}I_t + Z_{E,sx} * 0 + Z_{E,r}I_r}{Z_{E,E}}$$

$$\begin{bmatrix} V_t \\ \underbrace{V_{sx}}_{5\times1} \\ 0 \end{bmatrix} = \begin{bmatrix} Z'_{t,t} & \underbrace{Z'_{t,sx}}_{1\times5} & Z'_{t,r} \\ \underbrace{Z'_{sx,t}}_{5\times1} & \underbrace{Z'_{sx,sx}}_{5\times5} & \underbrace{Z'_{sx,r}}_{5\times1} \\ Z'_{r,t} & \underbrace{Z'_{r,sx}}_{1\times5} & Z'_{r,r} \end{bmatrix} \begin{bmatrix} I'_t \\ \underbrace{0}_{5\times1} \\ I'_r \end{bmatrix}$$

$$Z'_{t,t} = 2r_{DS} + R_t + \frac{1}{jw_sC_t} + jw_sL_t + \frac{w_s^2M_{t,E}^2}{R_E + jw_sL_E}$$

$$= 2r_{DS} + R_t + \underbrace{\frac{w_s^2M_{t,E}^2R_E}{R_E^2 + w_s^2L_E^2}}_{\substack{Added\ self \\ resistance}} + \frac{1}{jw_sC_t} + jw_s\left(L_t - \underbrace{\frac{w_s^2M_{t,E}^2L_E}{R_E^2 + w_s^2L_E^2}}_{\substack{Substracted\ self \\ inductance}}\right)$$

$$Z'_{t,r} = Z'_{r,t} = -jw_sM_{t,r} - \frac{w_s^2M_{t,E}M_{r,E}}{R_E + jw_sL_E}$$

$$= -\underbrace{\frac{w_s^2M_{t,E}M_{r,E}R_E}{R_E^2 + w_s^2L_E^2}}_{\substack{Introduced\ mutual \\ resistance}} - jw_s\left(M_{t,r} + \underbrace{\frac{w_s^2M_{t,E}M_{r,E}L_E}{R_E^2 + w_s^2L_E^2}}_{\substack{Added\ imaginary \\ term}}\right)$$

$$Z'_{t,sx} = \left[Z'_{t,sx}\right]^T = -jw_sM_{t,sx} + \frac{w_s^2M_{sx,E}M_{t,E}}{R_E + jw_sL_E}$$

$$= \underbrace{\frac{w_s^2M_{sx,E}M_{t,E}R_E}{R_E^2 + w_s^2L_E^2}}_{\substack{Introduced\ mutual \\ resistance}} - jw_s\left(M_{t,sx} - \underbrace{\frac{w_s^2M_{sx,E}M_{t,E}L_E}{R_E^2 + w_s^2L_E^2}}_{\substack{Substracted\ imaginary \\ term}}\right)$$

$$Z'_{r,sx} = \left[Z'_{sx,r}\right]^T = jw_sM_{r,sx} - \frac{w_s^2M_{sx,E}M_{r,E}}{R_E + jw_sL_E}$$

$$= -\underbrace{\frac{w_s^2M_{sx,E}M_{r,E}R_E}{R_E^2 + w_s^2L_E^2}}_{\substack{Introduced\ mutual \\ resistance}} + jw_s\left(M_{r,sx} + \underbrace{\frac{w_s^2M_{sx,E}M_{r,E}L_E}{R_E^2 + w_s^2L_E^2}}_{\substack{Added\ imaginary \\ term}}\right)$$

NAZARBAYEV UNIVERSITY

# Research Methodology and Modelling

Apply the same analysis performed for the system matrix of the system without EMO by deriving the equations for the sensing coil voltages $V_{s1}$, $V_{s2}$, $V_{s3}$, $V_{s4}$, $V_{s5}$ and inverter current $I_t$:

$$V_{sx} = I_t' Z_{sx,t}' + 0 * Z_{sx,sx}' + I_r' Z_{sx,r}' \qquad 0 = I_t' Z_{r,t}' + 0 * Z_{r,sx}' + Z_{r,r}' I_r' \qquad I_r' = -I_t' \frac{Z_{r,t}'}{Z_{r,r}'} \qquad V_{sx} = [V_{s1}, V_{s2}, V_{s3}, V_{s4}, V_{s5}]^T$$

$$V_{sx} = I_t' \left( \frac{Z_{sx,t}' Z_{r,r}' + Z_{r,t}' Z_{sx,r}'}{Z_{r,r}'} \right)$$

Using linear combinations of every sense coil voltage, first, simplify the equations by introducing geometric parameter $a_x$, where $x$ corresponds to each one of the open circuited sense coil voltages and then derive transmitter current $I_t$:

$$a_x' = \frac{Z_{sx,t}' Z_{r,r}' + Z_{r,t}' Z_{sx,r}'}{Z_{r,r}'} \qquad I_t' = \frac{1}{5} \sum_{i=1}^{5} V_{si} a_i' = \frac{1}{5} (V_{s1} a_1' + V_{s2} a_2' + V_{s3} a_3' + V_{s4} a_4' + V_{s5} a_5')$$

NAZARBAYEV UNIVERSITY

# ɔdology and Modelling

ɹgh 3-D eddy current FEA. In the simulation environment, the transmitter and receiver coils are excited
e from 10 kHz to 1 MHz and from 80 kHz to 90 kHz.

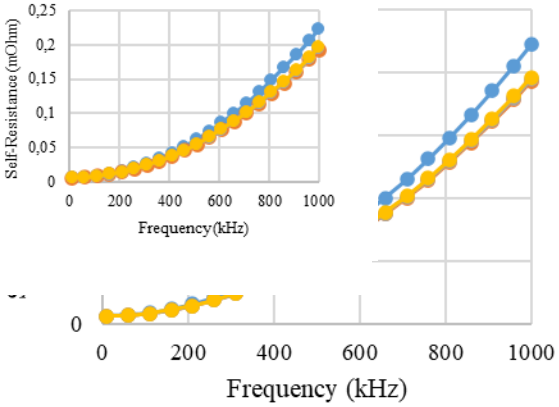


**Case 1**

No EMO

**Case 3**

Pressed tin can
*h*=82mm *r*=29.32mm

**Case 2**

100 KZT coin
*h*=1.9mm *r*=12.25mm

**Case 4**

Aluminum Spoon
*h*=0.92mm *l*=148mm

Fig 6. Four simulation cases in Ansys Electronics Desktop software.

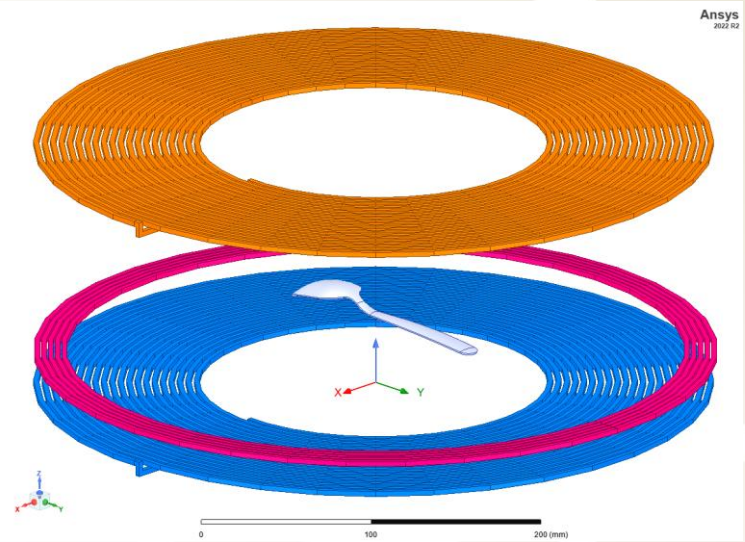


Fig 7. Simulation setup of the case 4 in the Ansys Electronics Desktop.

NAZARBAYEV UNIVERSITY

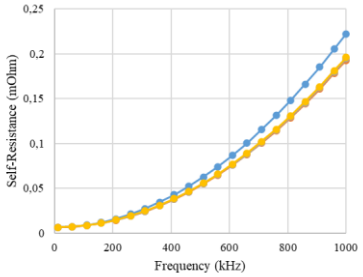


# Methodology and Modelling

ANSYS Electronics Desktop for the case of no EMO of the sense coil voltages and, self-inductances and resistances for the wide range of frequencies from 10 kHz to 1 MHz:

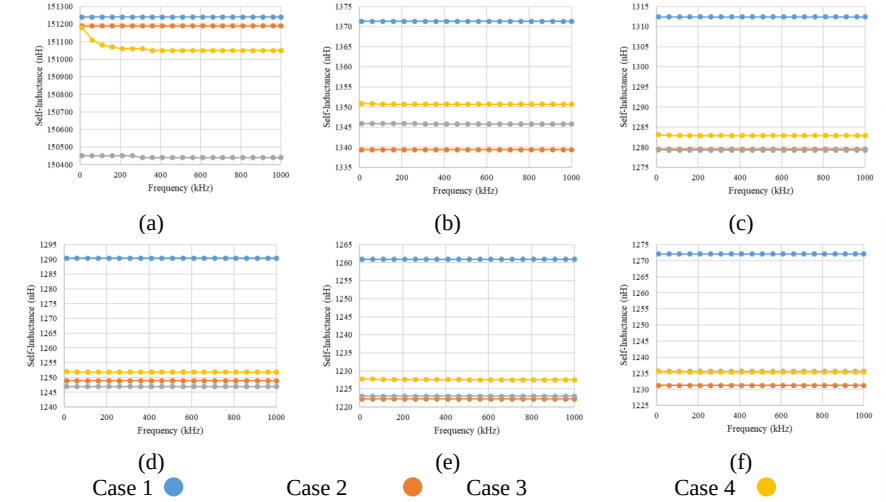


Fig 8. Self-inductance of (a) Transmitter coil, (b) S1 coil, (c) S2 coil, (d) S3 coil, (e) S4 coil, and (f) S5 coil over the range of frequency from 10 kHz to 1 MHz.

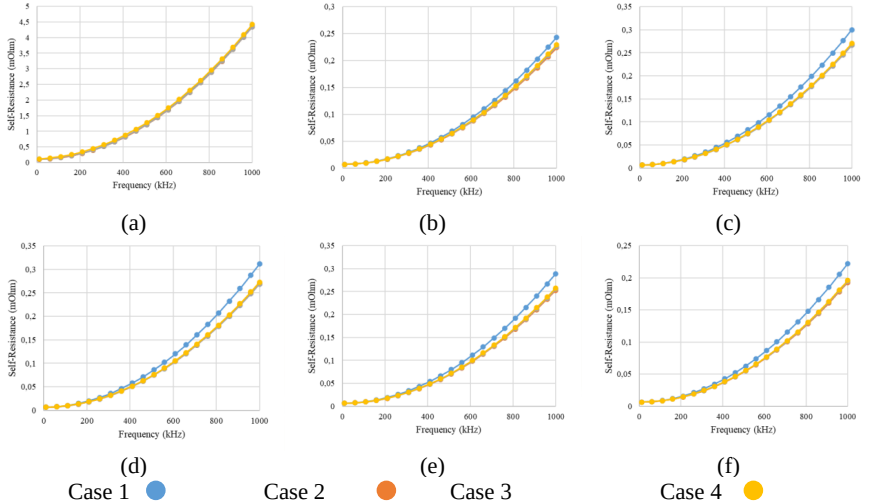


Fig 9. Self-resistance of (a) Transmitter coil, (b) S1 coil, (c) S2 coil, (d) S3 coil, (e) S4 coil, and (f) S5 coil over the range of frequency from 10 kHz to 1 MHz.

NAZARBAYEV UNIVERSITY

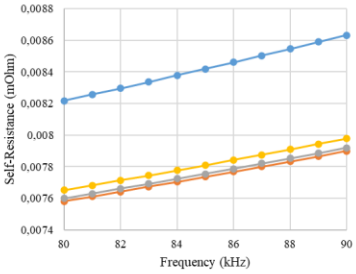


# Methodology and Modelling

rom 80 kHz to 90 kHz:

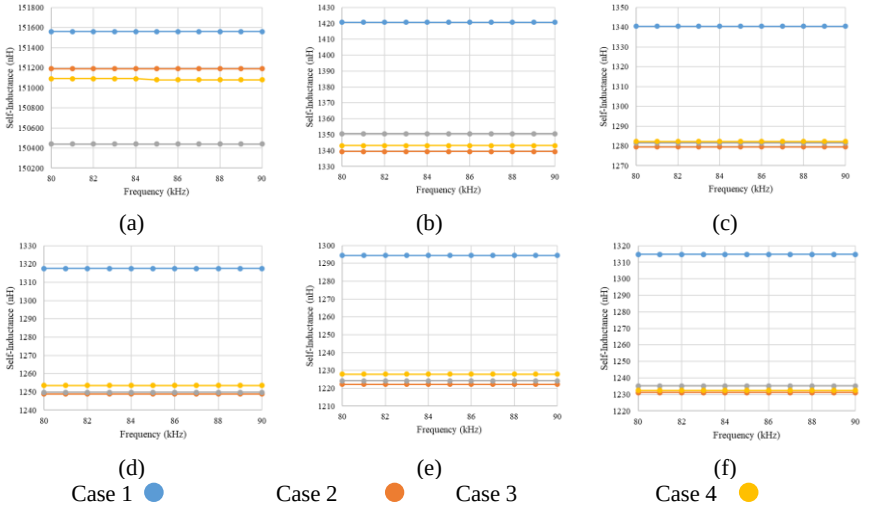


Fig 10. Self-inductance of (a) Transmitter coil, (b) S1 coil, (c) S2 coil, (d) S3 coil, (e) S4 coil, and (f) S5 coil over the range of frequency from 80 kHz to 90 kHz.

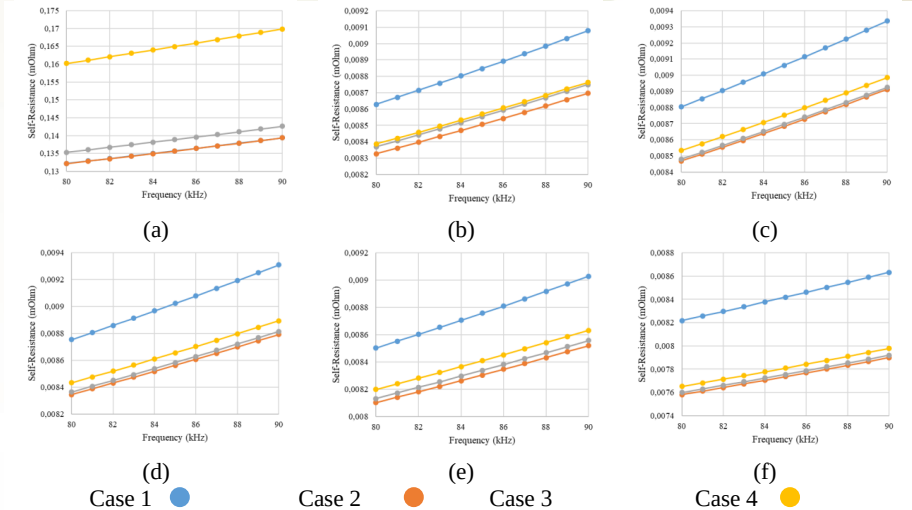


Fig 11. Self-resistance of (a) Transmitter coil, (b) S1 coil, (c) S2 coil, (d) S3 coil, (e) S4 coil, and (f) S5 coil over the range of frequency from 80 kHz to 90 kHz.

NAZARBAYEV UNIVERSITY

# Research Methodology and Modelling

Looking at the results of collecting data from the FEA technique, it can be seen that over the wide range of self-inductance of each coils stays the same, which shows that the self-inductance parameter of the coil itself is not dependent of the frequency at which the system operates, which is also shown in equation below:

$$L = \frac{N^2(D_i + N(D_w + s) - s)^2}{60(D_i + N(D_w + s) - s) - 44D_i}$$

This is Wheeler's high-accurate formula for computing self-inductance of a core-less flat spiral coils [11].

Another conclusion that we can make is that self-resistance parameter of the transmitter coil becomes higher in the presence of the EMO and it stays that way across the range of frequencies, whereas the sensing coils' self-resistance parameter becomes smaller in the presence of EMO with the very small change at the lower frequencies and higher change at the highest frequencies.

# Research Methodology and Modelling

Regarding the proposed methods ability of EOD across the range of frequencies. As the proposed method suggests, in order to obtain the geometric parameters $a_i$, they need to be calibrated in the base model of the system where no EMO is present. Using FEA technique, the data of the induced voltages in sense coils were collected across the wide range of frequencies. From the collected data across frequencies, which is labeled as n, the matrix for the voltage, a data vector for the current in transmitter coil, and a data vector for the geometric parameters are created:

$$V = \begin{bmatrix} V_1(f_1) & \cdots & V_5(f_1) \\ \vdots & \ddots & \vdots \\ V_1(f_n) & \cdots & V_5(f_n) \end{bmatrix} \qquad I_T = [I_T(f_1) \dots I_T(f_n)]^T \qquad a = [a_1\ a_2\ a_3\ a_4\ a_5]^T$$

After the parameters were established, the geometric parameters can be found using the method of least-squares:

$$a = (V^T V)^{-1} V^T I_T$$

# Research Methodology and Modelling

$a = [4.068754, 107.1975, 101.1746, -45.8134, -162.794]$

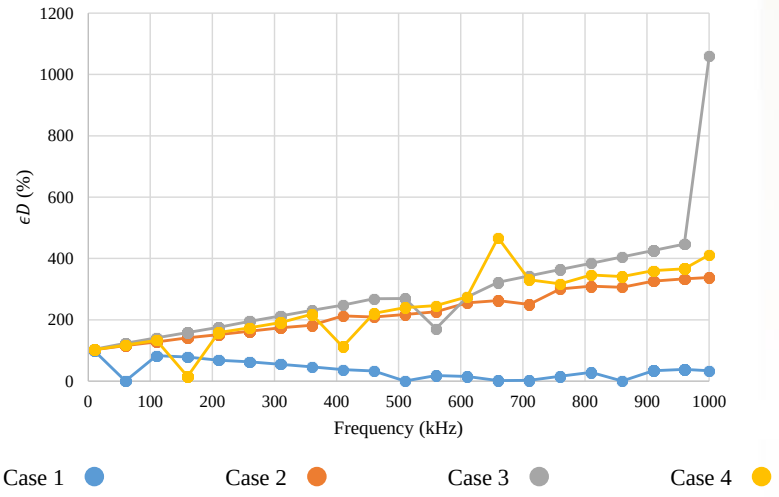


Fig 12. Sequent error results of the four simulation cases over the range of frequency from 10 kHz to 1 MHz.

$a = [419.2887, -492, 164.4657, 39.59464, -124.874]$

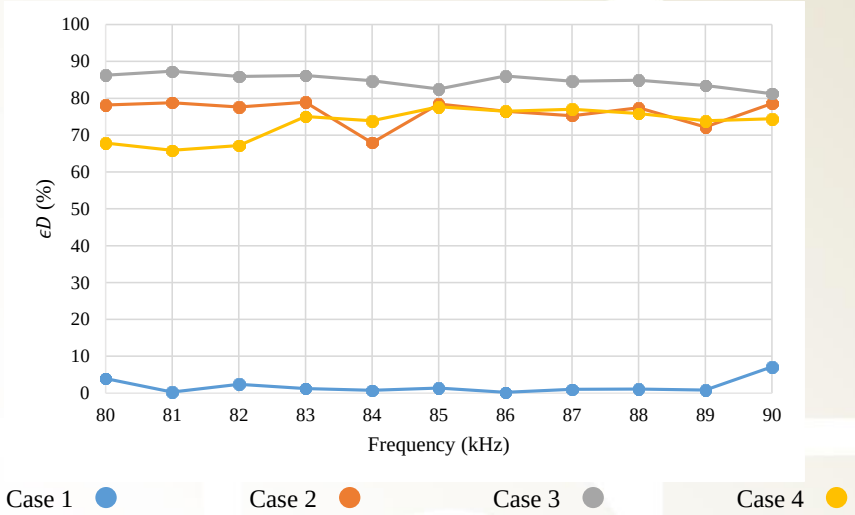


Fig 13. Sequent error results of the four simulation cases over the range of frequency from 80 kHz to 90 kHz.

# Experimental Setup

**Information on the setup**

The experimental setup for the proposed system is shown in Figure 4.1. The setup consists of 1) EL302RT Triple Power Supply device which serves a purpose of energizing the inverter with 12V and to be an input power source for the system; 2) Full-Bridge Inverter that transforms DC to AC; 3) Main setup that consists of transmitter, receiver and five open-circuited sensing coils; 4) Full-bridge rectifier circuit that transforms induced AC voltage and current in the receiver coil into DC; 5) BK PREDCISION 8600 DC Electronic Load modifying which system's imaginary load is created; 6) HDO8108R 1 GHz High Definition Oscilloscope is used to measure data from the sensing coil voltages and transmitter currents.

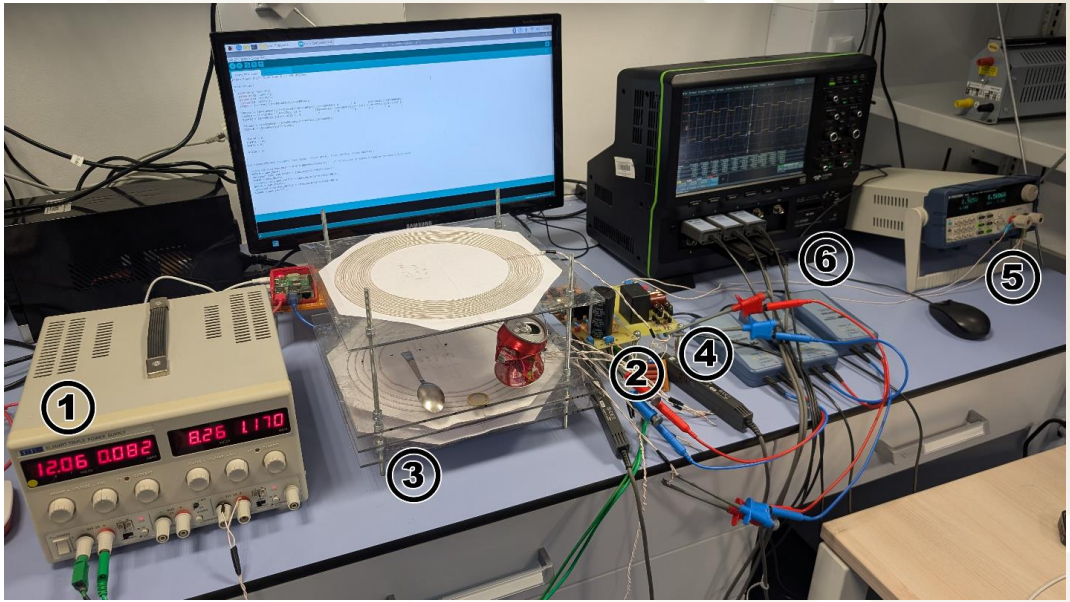


Fig 14. The experimental setup of the proposed system: 1) power supply; 2) inverter; 3) coil setup; 4) rectifier; 5) electronic load; 6) oscilloscope.

# Experimental Setup

**Case 1** No EMO

**Case 3**

Pressed tin can
$h$=8mm $r$31mm

**Case 2**

1 TRY coin
$h$=1.9mm $r$=13mm

**Case 4**

Aluminum Spoon
$h$=1.5mm $l$=144mm

Fig 15. Four experimental cases for the experimental setup.

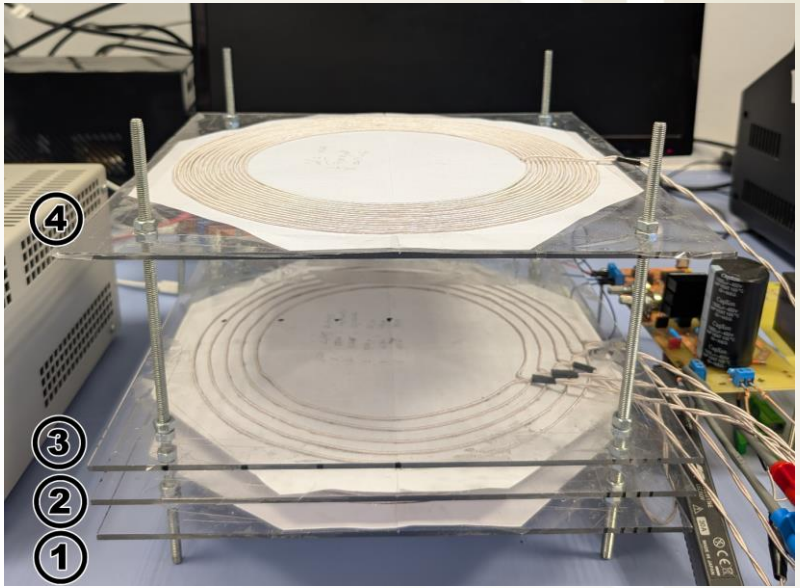


Fig 16. Coil setup of the proposed EOD method: 1) transmitter coil; 2) five open-circuited sensing coils; 3) space for EMO; 4) receiver coil.

# Experimental Setup

**Measurement of Coil Parameters**

Self-inductances and self-resistances of the transmitter and sensing coils in four cases in the frequency spectrum from 80 kHz to 90 kHz:

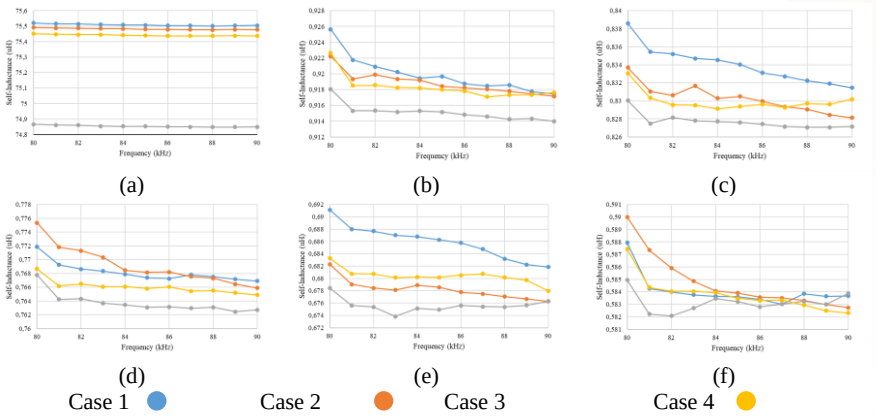


Fig 17. Measurement of self-inductance of (a) Transmitter coil, (b) S1 coil, (c) S2 coil, (d) S3 coil, (e) S4 coil, and (f) S5 coil over the range of frequency from 80 kHz to 90 kHz.

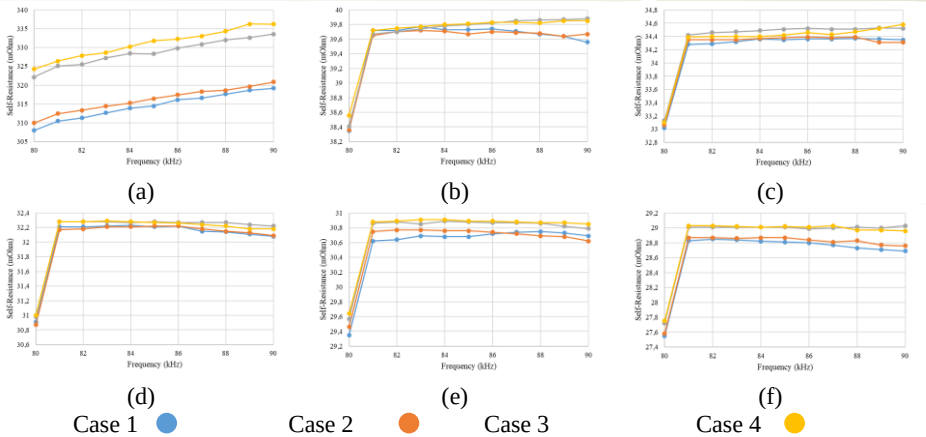


Fig 18. Measurement of self-resistance of (a) Transmitter coil, (b) S1 coil, (c) S2 coil, (d) S3 coil, (e) S4 coil, and (f) S5 coil over the range of frequency from 80 kHz to 90 kHz.

NAZARBAYEV UNIVERSITY

# Experimental Setup

**MOD at Constant Current and Constant Input Power Cases**

The next experimental procedure is to perform MOD over the frequency spectrum from 80 kHz to 90 kHz. In the case of experimental setup, due to technical reasons, it is unable to perform WPT over the spectrum of frequencies by managing to simultaneously maintain transmitter current of 2 A and input power level at 10 W:

$$a = [-5.232483625, -0.497182242, -2.097068643, 8.366829842, 1.352582627]$$

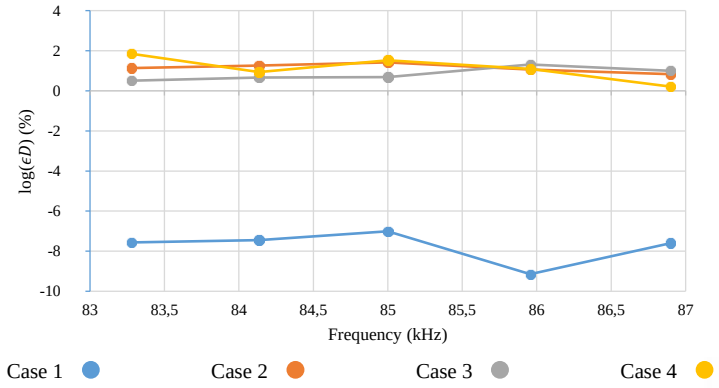


Fig 19. Sequent error results of the four experimental cases over the range of frequency from 80 kHz to 90 kHz at 2 A transmitter current.

$$a = [-0.40182235, 0.1431038, 0.0724854, 1.39473783, -0.58554156]$$

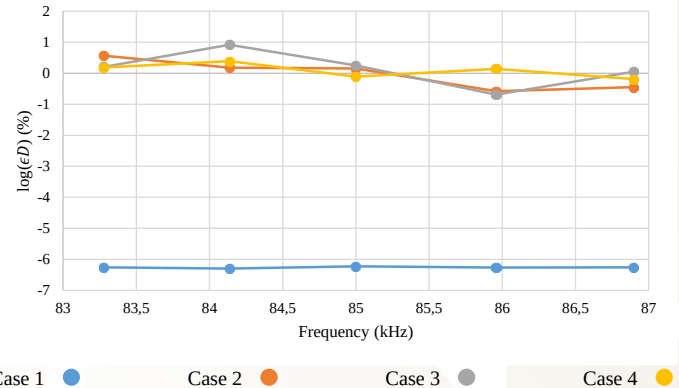


Fig 20. Sequent error results of the four experimental cases over the range of frequency from 80 kHz to 90 kHz at 10 W transmitter current.

# Experimental Setup

**Localization of the EMO**

Additional experimental procedures were performed in terms of localization of the EMO object at different heights and different locations from the center of the systems' operating area.

The reason for choosing specific points of height in the figure above is due to the usage of tin can as EMO for these experimental measurements and excessive heights levels are not possible. In the Table 4.1, the heatmap of the sequent error at the different points in the experimental setup and shown as:

Table 2. The sequent error values at different points of the experimental setup.

| $\epsilon D$ (%) | 0 cm | 3,75 cm | 7,5 cm | 11,25 cm | 15 cm |
|---|---|---|---|---|---|
| 6 cm | 0,613941 | 0,101289 | 1,410979 | 0,517403 | 1,372393 |
| 5 cm | 0,570676 | 0,393918 | 0,2314324 | 0,215687 | 0,186743 |
| 4 cm | 1,094192 | 1,075085 | 0,9843253 | 0,060868 | 1,152817 |

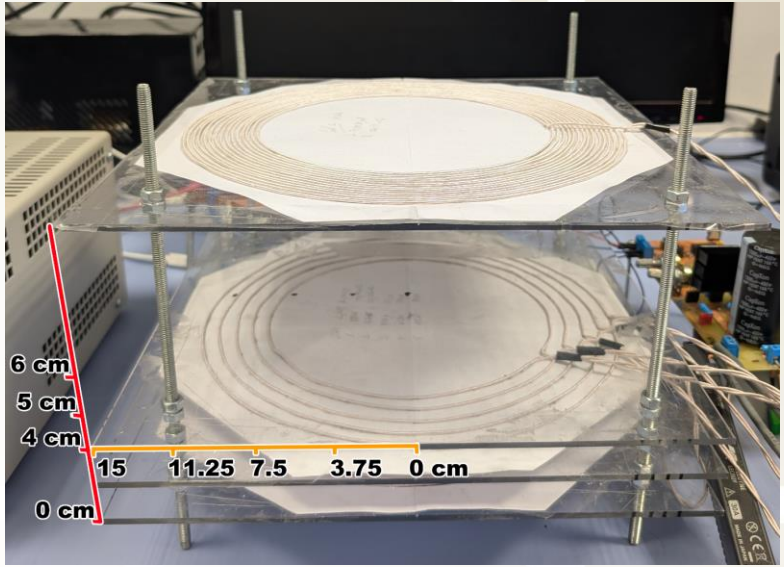


Fig 21. Different measuring points of the experimental setup for the localization purposes.

# Discussion

**MOD on the Frequency Spectrum**

- The sequent error for Case 1 in simulations at the frequency spectrum of 80-90 kHz was closer to 1 %, whereas in the cases with EMO displayed sequent errors in the range from around 70 % to 90 %, with the Case 3 being more detectable than the other cases.
- Over a wider frequency spectrum from 10 kHz to 1 MHz, the sequent error values of without EMO case is distinguishable yet non-reliable as in the other cases the sequent error linearly rises up to around 500 % with the outlier of around 1000 %.
- Constant transmitter current case being better compared to the constant power case.

**Sensitivity Analysis on the Parameters of the System**

- It is observed that the self-inductance of transmitter and five sensing coils demonstrated no frequency dependence.
- Regarding self-resistance values across the frequencies, it can be seen that due to the skin effect the value of it increase.
- the most change to the self-resistance values of transmitter coil is caused by the spoon, which consequently means that the more surface are the MO covers the higher its impact on the self-resistance value of the coils.

**Localization and Spatial Sensitivity**

- At the lowest height level, the sequent error values at the near center positions (0 cm and 3.75 cm) are higher than the values at higher heights.
- As the height becomes more, the sequent error values become higher the near edge positions (7.5 cm, 11.25 cm and 15 cm) than the values at the lower heights.

# Conclusion and Future Work

**Conclusion**

- Proposed a reliable sensing-coil system for EMO detection in WPT systems, addressing safety risks from overheating.
- Operates at low power (10 W) for pre-startup environmental scanning.
- Sequential error values effectively indicate EMO presence (1% without EMO, 70–90% with EMO).
- Narrow frequency range (80–90 kHz) ensures better stability and calibration.
- Spatial sensitivity highlights optimal detection zones based on EMO position.

**Future Work**

- Expand analysis on diverse EMO types (size, material).
- Improve system to distinguish harmless vs. hazardous objects.
- Explore detection performance with multiple EMOs.
- Implement real-time calibration for dynamic or post-calibration EMOs.
- Study environmental factors (dust, water) on EOD efficiency.

# Reference List

[1] P. Lopes, P. Costa and S. Pinto, "Wireless Power Transfer System For Electric Vehicle Charging," 2021 International Young Engineers Forum (YEF-ECE), Caparica / Lisboa, Portugal, 2021, pp. 132-137, doi: 10.1109/YEF-ECE52297.2021.9505094.
[2] S. A. Q. Mohammed and J. -W. Jung, "A Comprehensive State-of-the-Art Review of Wired/Wireless Charging Technologies for Battery Electric Vehicles: Classification/Common Topologies/Future Research Issues," in IEEE Access, vol. 9, pp. 19572-19585, 2021, doi: 10.1109/ACCESS.2021.3055027.
[3] S. Shafiei et al., "Design and Implementation of Underwater Inductive Power Transfer Systems with an Accurate Eddy Current Loss Model Approach," in IEEE Transactions on Industry Applications, doi: 10.1109/TIA.2024.3524480.
[4] A. Kapanov, A. Almaganbet, S. S. H. Yazdi and M. Bagheri, "Coil Parameters Optimization for Dynamic Wireless Charging of Electric Vehicles using Particle Swarm Optimization (PSO) Algorithm," 2023 International Aegean Conference on Electrical Machines and Power Electronics (ACEMP) & 2023 International Conference on Optimization of Electrical and Electronic Equipment (OPTIM), Istanbul, Turkiye, 2023, pp. 1-7, doi: 10.1109/ACEMP-OPTIM57845.2023.10287037.
[5] H. Jiang, P. Brazis, M. Tabaddor and J. Bablo, "Safety considerations of wireless charger for electric vehicles — A review paper," 2012 IEEE Symposium on Product Compliance Engineering Proceedings, Portland, OR, USA, 2012, pp. 1-6, doi: 10.1109/ISPCE.2012.6398288.
[6] R. Wiengarten, V. Reising, T. Vosshagen and F. Turki, "About the heating of foreign metallic objects in magnetic field of wireless power transfer by cars," Proceedings of PCIM Europe 2015; International Exhibition and Conference for Power Electronics, Intelligent Motion, Renewable Energy and Energy Management, Nuremberg, Germany, 2015, pp. 1-5.
[7] S. Y. Chu, X. Zan and A. -T. Avestruz, "Electromagnetic Model-Based Foreign Object Detection for Wireless Power Transfer," in IEEE Transactions on Power Electronics, vol. 37, no. 1, pp. 100-113, Jan. 2022, doi: 10.1109/TPEL.2021.3100420.
[8] S. Y. Chu and A. -T. Avestruz, "Transfer-power measurement: A non-contact method for fair and accurate metering of wireless power transfer in electric vehicles," 2017 IEEE 18th Workshop on Control and Modeling for Power Electronics (COMPEL), Stanford, CA, USA, 2017, pp. 1-8, doi: 10.1109/COMPEL.2017.8013344.
[9] A. Rakhymbay, M. Bagheri and M. Lu, "A simulation study on four different compensation topologies in EV wireless charging," 2017 International Conference on Sustainable Energy Engineering and Application (ICSEEA), Jakarta, Indonesia, 2017, pp. 66-73, doi: 10.1109/ICSEEA.2017.8267689.
[10] J. P. K. Sampath, A. Alphones and D. M. Vilathgamuwa, "Repeater tuning against load variation for wireless power transfer," 2016 IEEE 8th International Power Electronics and Motion Control Conference (IPEMC-ECCE Asia), Hefei, China, 2016, pp. 3173-3177, doi: 10.1109/IPEMC.2016.7512803.
[11] K. Aditya and S. S. Williamson, "Design Guidelines to Avoid Bifurcation in a Series–Series Compensated Inductive Power Transfer System," in IEEE Transactions on Industrial Electronics, vol. 66, no. 5, pp. 3973-3982, May 2019, doi: 10.1109/TIE.2018.2851953.

# Thank You for Your Attention!

# Q&A